

**AN INVESTIGATION ON THE MIXING DYNAMICS OF A
CHANNEL-TYPE MICROCOMBUSTOR**

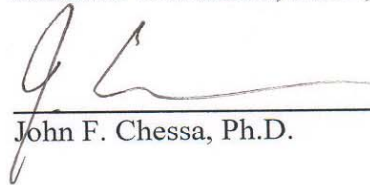
IVAN ALEJANDRO ANCHONDO

Department of Mechanical and Industrial Engineering

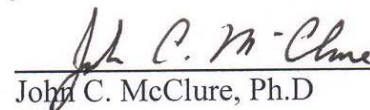
APPROVED:



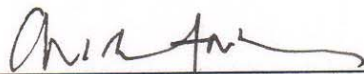
Ahsan R. Choudhuri, Ph.D., Chair



John F. Chessa, Ph.D.



John C. McClure, Ph.D.



Charles H. Ambler, Ph.D.
Dean of the Graduate School

**INVESTIGATION ON THE MIXING DYNAMICS OF A
CHANNEL-TYPE MICROCOMBUSTOR**

by

IVAN ALEJANDRO ANCHONDO, B.S.M.E.

THESIS

Presented to the Faculty of the Graduate School of
The University of Texas at El Paso

in Partial Fulfillment
of the Requirements

for the Degree of

MASTER OF SCIENCE

Department of Mechanical and Industrial Engineering

THE UNIVERSITY OF TEXAS AT EL PASO

December, 2003

UMI Number: EP10511

PREVIEW

UMI[®]

UMI Microform EP10511

Copyright 2003 by ProQuest Information and Learning Company.

All rights reserved. This microform edition is protected against
unauthorized copying under Title 17, United States Code.

ProQuest Information and Learning Company
300 North Zeeb Road
PO Box 1346
Ann Arbor, MI 48106-1346

Executive Summary

This thesis delineates an investigation in the mixing behavior of methane and air inside a channel type microcombustor. The geometry studied was 40 mm long, 5 mm high, and 5 mm wide, and all inlets were 1.9 mm in diameter. Two simple 2D structured grid configurations were simulated for their laminar and turbulent flows, at lean, stoichiometric, and rich conditions to formulate the initial understanding on the mixing qualities of the chamber. It was determined that mixing occurred by diffusion as methane and air interacted at their boundary and by the chaotic trajectories developed at the impingement point of two vertical air jets. Six more multiple inlet 2D structured grid configurations were developed and studied at laminar conditions only. A most efficient configuration was obtained and studied at its lean, stoichiometric, and rich mixture conditions. This configuration was composed by a combination of the two mixing initiators observed from the previous step of the investigation. This design consisted of five inlets: air was injected through the second set of vertical inlets and an axial one, while methane was injected through the first set of vertical ports. This configuration was also analyzed in a 3D unstructured grid domain. This design was characterized by a high pressure region where the inlets were located, a high concentration of methane at the corners, and an acceleration of the flow passed the impinging vertical air jets. Mixing occurred by the interaction of fuel and air around the axial air jet and as result of local turbulence and vortices created by the colliding jets. The Equivalent ratios at the second half of the chamber in all three mixture conditions suggested that if ignition and

combustion are possible within this cavity, it will occur there, in the second portion of the chamber. The second half of the chamber demonstrated a uniform distribution of methane all around and lower flow velocities. It is concluded that this configuration has great potential for ignition and combustion inside the chamber volume, at least from a mixing perspective.

PREVIEW

Table of Contents

EXECUTIVE SUMMARY	i
TABLE OF CONTENTS	iii
NOMENCLATURE	vi
LIST OF TABLES	viii
LIST OF FIGURES	x
CHAPTER 1. INTRODUCTION	1
1.1 Objectives	4
1.2 Project Overview	4
1.3 Organization of Thesis	6
CHAPTER 2 LITERATURE REVIEW	7
2.1 Microheat Power Generators	7
2.2 Microcombustion Processes	9
2.2.1 Mixing	9
2.2.2 Ignition	11
2.2.3 Stability	14
2.3 Mixing Inside Microgeometries	17
CHAPTER 3 NUMERICAL METHODS	18
3.1 Governing Equations	19
3.1.1 Continuity Equation	20
3.1.2 Momentum Equation	22
3.1.3 Energy Equation	25
3.2 Turbulent Modeling	27
3.2.1 Turbulence Model $k-\epsilon$	29
3.3 Discretization Method	31

3.3.1	Convective Discretization	33
3.3.1.1	Upwind Scheme	34
3.3.2	Diffusion Discretization	35
3.3.3	Source Term Linearization	37
3.3.4	Finite Difference Equation	38
3.4	Solution Algorithm	39
3.5	Unstructured Grid	43
3.5.1	Discretization of Convection-Diffusion Equation	45
3.6	Model Grid	50
CHAPTER 4	RESULTS	53
4.1	2D Tri-Inlet Configuration	55
4.1.1	2D Laminar Simulations	56
4.1.2	2D Turbulent Simulations	69
4.2	2D Multiple-Inlet Configuration	72
4.3	3D Multiple-Inlet Configuration	85
4.3.1	Pressure	87
4.3.2	U-velocity	94
4.3.3	V-velocity	101
4.3.4	Vorticity	108
4.3.5	Methane Mass Fraction	116
CHAPTER 5	CONCLUSIONS AND RECOMMENDATIONS	124
5.1	2D Final Configuration	124
5.2	3D Final Configuration	125
5.3	Recommendations for Future Work	127
REFERENCES	129
Appendix A:	MODULE SIMULATION INFORMATION	132
Appendix B:	PROCEDURE TO OBTAIN AF_{ACTUAL}	135
Appendix C:	2D TRI-INLET PRELIMINARY CASES DATA PROFILES.	136

Appendix D: 2D TRI-INLET SIMULATIONS PROFILES.....	148
Appendix E: 2D TRI-INLET TURBULENT SIMULATIONS	136
Appendix F: 2D INITIAL MULTIPLE-INLET SIMULATION PROFILES.....	159
Appendix G: 3D MULTIPLE-INLET SIMULATION PROFILES	165
Appendix H: EQUIVALENT RATIOS AT THE 2ND HALF OF CHAMBER	195
Appendix I: EXPERIMENT	196
Curriculum Vitae	198

PREVIEW

Nomenclature

English

A	Area
a_x	Acceleration in the x-direction
AF	Air-Fuel Ratio
C	Constant
$C_{\varepsilon 1}$	Coefficient of production of ε in ε -equation
$C_{\varepsilon 2}$	Coefficient of destruction of ε in ε -equation
C_u	Coefficient in the eddy viscosity relation in k- ε model
c_v, c_p	Specific heat
D	Diameter
E	Energy of the system
E	Eastern node in the discretized control volume
e	Internal energy
\hat{e}	Unit vector
F	Force
F_x	Force exerted in the x-direction
g	Gravitational Constant
h	Static enthalpy
J_f	Mass flow rate
k	Thermal Conductivity
k	Turbulent kinetic energy
l	Length scale
ℓ	Length
L	Characteristic length
m	Mass
MW	Molecular weight
N	Northern node in the control discretized volume
P	Pressure
P	Center node in the discretized control volume
Q'''	Volumetric heat release
r	Radius
R	Gas' constant
R_u	Universal gas constant
Re	Reynolds number
S	Southern node in the control discretized volume
S	Source term
T	Temperature
t	Time
T_i	Turbulent intensity
u	Cartesian component of velocity in x-direction

U	Velocity in x-direction (simulation data)
\tilde{u}	Time averaged mean velocity
\mathbf{V}	Velocity vector containing all three velocity components
$ \mathbf{V} $	Velocity magnitude
V	Velocity in the y-direction (simulation data)
V	Volume
v	Cartesian component of velocity in y-direction
w	Cartesian component of velocity in z-direction
\mathbf{W}	Western node in the discretized control volume
W	Work done on or by the system
x	Cartesian coordinate
X	Chamber axial distance
y	Cartesian coordinate

Greek

Φ	Equivalence ratio
δ	Flame thickness
α	Thermal conductivity
Ω	Angular velocity
ω	Vorticity
ρ	Density
μ	Molecular (laminar) dynamic viscosity
Γ	Diffusion coefficient
Γ_t	Turbulent diffusivity coefficient
ε	Rate of turbulence dissipation
ε_{res}	Residuals
ν	Kinematic viscosity
\mathcal{V}	Velocity scale
μ	Dynamic viscosity
η	Computational coordinate
ξ	Computational coordinate
ϕ	General scalar flow variable
τ	Shear stress
σ	Normal stress
μ_t	Eddy (turbulent) dynamic viscosity
∇	Vector operator

List of Tables

Table 4.1. 2D Tri-inlet preliminary case studies.	55
Table 4.2. Configuration I: U-velocity	61
Table 4.3. Configuration II: U-velocity	61
Table 4.4. Configuration I: V-velocity	62
Table 4.5. Configuration II: V-velocity	62
Table 4.6. Configuration I: Pressure (gauge)	63
Table 4.7. Configuration II: Pressure (gauge)	63
Table 4.8. Configuration I: CH ₄ Mass Concentration	64
Table 4.9. Configuration II: CH ₄ Mass Concentration	64
Table 4.10. Configuration I: Laminar vs. Turbulent CH ₄ concentration. (Centerline data)	70
Table 4.11. Configuration II: Laminar vs. Turbulent CH ₄ concentration. (+1 data)	72
Table 4.12 Configuration VI: Inlet velocities	77
Table 4.13. Configuration VI: U- velocity	79
Table 4.14. Configuration VI: V- velocity	81
Table 4.15. Configuration VI: Pressure (gauge)	83
Table 4.16. Configuration VI: CH ₄ Mass Concentration	85
Table 4.17. 3D Simulations detailed information	86
Table 4.18. 3D Multiple-Inlet Configuration (Stoichiometric): Pressure	92
Table 4.19. 3D Multiple-Inlet Configuration (Lean): Pressure	93
Table 4.20. 3D Multiple-Inlet Configuration (Rich): Pressure	93
Table 4.21. 3D Multiple-Inlet Configuration (Stoichiometric): U-Velocity	99
Table 4.22. 3D Multiple-Inlet Configuration (Lean): U-Velocity	99
Table 4.23. 3D Multiple-Inlet Configuration (Rich): U-Velocity	100
Table 4.24. 3D Multiple-Inlet Configuration (Stoichiometric): V-Velocity	106

Table 4.25. 3D Multiple-Inlet Configuration (Lean): V -Velocity	106
Table 4.26. 3D Multiple-Inlet Configuration (Rich): V -Velocity	107
Table 4.27. 3D Multiple-Inlet Configuration (Stoichiometric): Vorticity Ratio	114
Table 4.28. 3D Multiple-Inlet Configuration (Lean): Vorticity Ratio	114
Table 4.29. 3D Multiple-Inlet Configuration (Rich): Vorticity Ratio	115
Table 4.30. 3D Multiple-Inlet Configuration (Stoichiometric): CH_4 Concentration	121
Table 4.31. 3D Multiple-Inlet Configuration (Lean): CH_4 Concentration	121
Table 4.32. 3D Multiple-Inlet Configuration (Rich): CH_4 Concentration	122

List of Figures

Figure 3.1. Fluid element of volume $dx dy dz$ with mass fluxes through various Faces	20
Figure 3.2. Forces in the x-direction acting on the faces of fluid element	23
Figure 3.3. Control volume for a two-dimensional grid.	32
Figure 3.4. Discretized domain used in the upwind scheme with flow entering the control volumes a) positive flow b) negative flow.	35
Figure 3.5. Discretized domain with control volume.	36
Figure 3.6. Solution flowchart for the SIMPLEC algorithm.	42
Figure 3.7. Structured (left) and Unstructured (right) mesh	43
Figure 3.8. Thin-layered tetrahedral (Δn_1 - height of first node, Δn_c - height of cell centroid).	43
Figure 3.9. Reconstruction stencil for tetrahedral cell-based scheme.	45
Figure 3.10. Structured grid control volume	46
Figure 3.11. Tri-Inlet and Multiple Inlet 2D computational domain.	50
Figure 3.12. 3D Unstructured Grid Domain.	51
Figure 3.13. CH_4 stoichiometric simulation grid optimization comparison between max cell size = 0.5 (a) and a max cell size = 0.3 (b)	52
Figure 4.1. a) Configuration I b) Configuration II.	55
Figure 4.2. a) $\Phi=0.504$ b) $\Phi=0.714$ c) $\Phi=1.0$ d) $\Phi=1.429$ e) $\Phi=2.389$ f) $\Phi=3.846$	57
Figure 4.3. Stoichiometric Pressure Profile. Top: Configuration I Bot: Configuration II.	58
Figure 4.4. Stoichiometric U-velocity Profile. Top: Configuration I Bot: Configuration II.	58

Figure 4.5. <i>Stoichiometric V-velocity Profile. Top: Configuration I</i>	
<i>Bot: Configuration II.</i>	59
Figure 4.6. <i>Stoichiometric CH₄ Mass Concentration Profile. Top: Configuration I</i>	
<i>Bot: Configuration II.</i>	59
Figure 4.7. <i>Horizontal Data Slices.</i>	60
Figure 4.8. <i>Configuration I- Lean: High CH₄ concentration region.</i>	65
Figure 4.9. <i>Configuration I- Rich: CH₄ jet penetrating impingement point.</i>	67
Figure 4.10. <i>Configuration II- Rich: CH₄ mass concentration.</i>	69
Figure 4.11. <i>Configuration II: Comparison of the CH₄ mass fraction</i> <i>between the stoichiometric laminar (top) and the stoichiometric</i> <i>turbulent (bot) simulations.</i>	71
Figure 4.12. <i>2D Multiple Inlet Configurations.</i>	74
Figure 4.13. <i>2D Multiple Inlet Configurations CH₄ mass concentrations.</i>	76
Figure 4.14. <i>Configuration VI: U-velocity Profile a) Stoichiometric b) Lean</i> <i>c) Rich.</i>	78
Figure 4.15. <i>Configuration VI: V-velocity Profile a) Stoichiometric b) Lean</i> <i>c) Rich.</i>	80
Figure 4.16. <i>Configuration VI: Pressure Profile a) Stoichiometric b) Lean</i> <i>c) Rich.</i>	82
Figure 4.17. <i>Configuration VI: CH₄ Mass Fraction Profile a) Stoichiometric</i> <i>b) Lean c) Rich.</i>	84
Figure 4.18. <i>3D Simulation Data Horizontal Slices and Vertical Cuts.</i>	86
Figure 4.19. <i>Stoichiometric Pressure profile: Impingement point with U-velocity</i> <i>vectors.</i>	87
Figure 4.20. <i>3D Stoichiometric Pressure Profile.</i>	89
Figure 4.21. <i>3D Lean Pressure Profile.</i>	90
Figure 4.22. <i>3D Rich Pressure Profile.</i>	92
Figure 4.23. <i>3D Stoichiometric U-velocity Profile.</i>	95

Figure 4.24. 3D Lean U-velocity Profile	97
Figure 4.25. 3D Rich U-velocity Profile.	98
Figure 4.26. Stoichiometric velocity profile and vectors backflow and recirculation areas near the inlets.	101
Figure 4.27. 3D Stoichiometric V-velocity Profile.	102
Figure 4.28. 3D Lean V-velocity Profile.	104
Figure 4.29. 3D Rich V-velocity Profile.	105
Figure 4.30. Vorticity profile and velocity vectors at air jet's impingement.	109
Figure 4.31. 3D Stoichiometric Vorticity Profile.	110
Figure 4.32. 3D Lean Vorticity Profile.	112
Figure 4.32. 3D Rich Vorticity Profile.	113
Figure 4.34. 3D Stoichiometric CH ₄ Concentration Profile.	117
Figure 4.35. 3D Lean CH ₄ Concentration Profile.	119
Figure 4.36. 3D Rich CH ₄ Concentration Profile.	120

Chapter 1

INTRODUCTION

The rapid progress in microfabrication technologies has made possible the development of microscale energy conversion devices commonly known as Power Micro Electro-Mechanical System (Power MEMS). Due to the higher energy density of hydrogen and hydrocarbon fuels, combustion process based miniature power generators (microengines, microgasturbines, microrockets, etc.) have the potential to be more compact and longer-lived than chemical batteries and, as a result, will be critical for portable power source applications. For example, hydrocarbon fuels provide an energy density of typically 45 MJ/kg, whereas even modern lithium ion batteries commonly used in laptop computers provide only about 0.50 MJ/kg. Thus even at only 10% conversion efficiency from thermal to electrical energy, hydrocarbon fuels provide 10 times higher energy storage density than batteries. Additionally, using a simple one-dimensional analysis it can be shown that the energy density of a thrust-producing device increases as its size decreases (*Schilp*). Thus, the development process of subkilogram class missile interceptors and microspacecrafts will also greatly benefit from the advancement of Power MEMS based propulsion systems. However, successful miniaturization of combustors components demands a more complete and broader understanding of microfluid dynamics and microcombustion phenomena. It is not clear whether or not the presently available theories and databases are adequate to predict the combustion

behavior and flow dynamics in millimeter or submillimeter-scale systems. While flame propagation at the microscale is feasible, the interplay of fluid dynamics, kinetics and transport in flame stability and combustion characteristics of these systems is poorly understood. The traditional view is that combustion processes do not scale to smaller sizes well. Essentially, this becomes an issue of residence time. If the time required for combustion is larger than the time any given quantity of fuel resides in the chamber, the combustion will be incomplete and the engine will suffer a performance penalty. The rates of combustion reactions are independent of scale, so if they represent the limit that sets the residence time, it would not be possible to effectively scale combustion engines to small sizes. Also continuum theory predicts that a critical diameter (in the millimeter length scale) is necessary for propagation of an exothermic reaction (*Lewis, Kuo*). These theories, which compare fairly well with experimental data, focus on the competition between heat loss from the flame front to the cold boundary and heat generation from the chemical reaction. In contrast, recent experiments (*Faulkner, Janson, Choudhuri*) clearly indicate that propagation in a microchannel is quite feasible. However, there is another factor to consider. In order for these reactions to take place, the fuel and the oxidizer must be in close proximity and this can be accomplished through injection and mixing in the chamber. In fact, this process typically occupies the majority of the time a fuel element spends in a combustion chamber. This is a primarily fluid dynamic process, and it does scale. But in practice turbulent mixing is not readily available when the channel Reynolds number is small. On the other hand, laminar mixing through molecular

diffusion is too slow and therefore impractical in many cases. As posted in recent studies (*Evans, Lee 1999, Volpert, Lee 2000*) the onset of chaotic trajectories may be a way to obtain mixing in laminar micro-flows. Data such as local velocities and fuel mixture fractions are crucial to the design of these combustor geometries and mixing schemes. Thus, the understanding the fuel-air mixing process is crucial to develop microcombustors capable of burning hydrogen or hydrocarbon fuels.

Motivated by the foregoing issues, the Combustion and Propulsion Research Laboratory (CPRL) at the University of Texas at El Paso (UTEP) has embarked on the challenge of understanding the mixing behavior of a Channel-Type microcombustor¹.

The Combustion and Propulsion Research Laboratory is located in the Mechanical and Industrial Engineering Department. The laboratory possesses the facilities and software to conduct research on fundamental mixing and combustion characteristics of microcombustion components. The research of focus conducted in the CPRL includes micropropulsion, microcombustion, and microgravity combustion. Direct injection spark ignition engine research, gas turbine combustors, and intelligent active combustion control are other projects performed in the CPRL.

¹ The term 'micro' used here does not link the combustor dimension exactly to the micron scale, but refers to the dimension of a conventional combustor. A microfabricated gas turbine with a power rating of 10 W will have a 2mm combustor intake diameter, which is 1/1000 of the combustor intake (~2 m) of a typical gas turbine combustor

1.1 Objectives

The overall objective of this research was to numerically investigate the mixing behavior of the laminar flow inside an 8:1 (length to diameter) ratio channel-type microcombustion chamber. In order to design an efficient chamber configuration, different fuel and air injector arrangements were studied for acceptable entrainment of fuel and air at their lean, rich, and stoichiometric compositions. The objectives of this thesis were:

1. To design by numerical computation an efficient fuel and air injector configuration in a two-dimensional microcombustion chamber domain.
2. To numerically study the side wall effect, in the three-dimensional domain, of the injector configuration obtained from the 2D investigation.

1.2 Project Overview

The project was divided into three phases to accomplish the research objectives. Each phase depended on the previous one. The phases began with the comprehension and analysis of the fluid dynamic characteristics of simple air/fuel jet arrangements.

- 2D Tri-Inlet Configuration: This segment of the design consisted of a numerical analysis of a 2-dimensional 5mm high and 40 mm long channel type combustion chamber with a three inlet configuration and two air/fuel jet arrangements. The study was aimed at understanding the effects of the two air and fuel inlet configurations on the mixing behavior inside the microchamber at lean, rich, and

stoichiometric mixtures. Laminar flow through the chamber cavity was solved by the compressible Navier-Stokes equations over the two dimensional computational domain.

- **2D Multiple-Inlet Configuration:** Once there was a solid understanding on the role played by the air and fuel inlet configuration on the local mixing, the next step was to design a two-dimensional chamber with multiple arrangements of four, five, and more inlets and observe the mixing behavior of each configuration at their lean, rich, and stoichiometric concentrations. This part of the study was aimed at obtaining an inlet configuration that could produce significant mixing to support and maintain ignition within its small volume. Laminar flow through the chamber cavity was solved by the compressible Navier-Stokes equations over the two dimensional computational domain.
- **3D Multiple-Inlet Configuration:** The most efficient design chosen from the previous study was numerically analyzed as a three-dimensional model to obtain more accurate results on the true mixing characteristics of this inlet configuration. Laminar flow through the chamber cavity was solved by the compressible Navier-Stokes equations over the three dimensional computational domain. This final part of the investigation provided further insight into the real life application mixing behavior and will assist into further design alternatives such as blunt bodies or sudden stepping.

1.3 Organization of Thesis

The approach utilized to accomplish the objectives of this thesis, discussion, results obtained, and conclusions are broken down into five chapters. Chapter 2 provides and insight into microheat power generators, microcombustion processes, and mixing inside microgeometries. Chapter 3 contains the derivation of the governing equations, and the numerical methods used in the discretization of equations for 2D and 3D domains, as well as the grid generation process. The results and discussions of each of the different numerical simulations are presented in Chapter 4. Chapter 4 is divided into three sections. Section 4.1 discusses the 2D Tri-Inlet Configuration part of the investigation; section 4.2 talks about the 2D Multiple-Inlet Configuration; and section 4.3 presents the 3D Simulation of a highly efficient configuration obtain from section 4.2. The thesis is finalized with conclusions and recommendations in Chapter 5. Finally, appendices provide visual information of all the cases studied in this thesis.

Chapter 2

LITERATURE REVIEW

This chapter contains the necessary background relevant to this research. The chapter begins with an introduction to microheat power generators. The chapter then moves on to the discussion microcombustion processes which is broken down into three sections: mixing, stability, and ignition. Finally, the mixing behavior inside microgeometries is discussed. Interested readers may refer to literature pertaining to combustion, microcombustion, MEMS, and micromixing for further information.

2.1 Microheat Power Generators

It is well known that the use of combustion processes for electrical power generation provides enormous advantages over batteries in terms of energy storage per unit mass (40 MJ/kg vs. 0.5 MJ/kg) and in terms of power generation per unit volume. Microburners are emerging as a powerful tool for portable production of energy that may soon replace expensive and environmentally unfriendly lithium batteries in laptops, cellular phones, and other communication devices. Still, these advantages of combustion processes have not yet been exploited to their full electrical power generation potential in these small-scale systems.

Most current microscale combustion generator concepts employ scale down versions of existing macroscale devices, the problem is that this microdevices experience

more problems with heat loss, friction, sealing, fabrication, and assembly than their macro counterparts. For this reason, it seems that a power source with no moving parts and no precision fabrication and assembly such as heat-recirculating or channel-type combustors are the best option.

Attempts at understanding the behavior of microcombustor devices has been approached by many researchers as the use for this technology ranges from industry and military applications to civilian personal use. Research on recirculating or swiss roll combustor indicate that combustion in this microscale combustion devices at low Reynolds number is possible, but require heat recirculation as well as catalytic combustion (*Sitski*). Other studies in microchannel mixing and combustion suggest that stable combustion can be achieved by sudden step, also useful in controlling the position of the flame (Yang), and that mixing in micro laminar flows can be enhanced by the onset of chaotic trajectories (*Lee 2000*).

The inability to perform detailed analysis in this microscale structures as well as the expensive turnaround of minor changes during experimentation make numerical modeling a useful tool when seeking to understand the mixing and combustion behavior of microheat power generators. Two-dimensional and three-dimensional computational fluid dynamics models allow researchers to observe the phenomena inside these small configurations, and along with detail transport, chemistry, and proper interfacial boundary conditions, emerge with initial theories and ways to improve their systems.

2.2 Microcombustion Processes

The rapid progress in fabrication and utilization of micro-electromechanical systems and the interest in microcombustion power generators have not been matched by the corresponding advances in our understanding of the unconventional flow and combustion physics of such devices. This section explores the known behavior on the mixing, stability, and ignition of microcombustion processes.

2.2.1 Mixing

Fluid flows in small devices differ from those in macroscopic machines. The operation of MEMS-based ducts cannot always be predicted from conventional flow models such as the Navier–Stokes equations with no-slip boundary condition at a fluid–solid interface, as routinely and successfully applied for larger flow devices. Nevertheless, the current numerical models may be the only way to perform initial analysis on the flow dynamics in microstructures.

Mixing of fuel and air is one of the important considerations for the design of microcombustion systems. The mixing efficiency of the fuel and air jets in combustors is an important factor in their overall performance, where reductions in their size and weight will be possible if the mixing can be improved. Mixing occurs as the boundaries of the fuel and air interact with each other. Jets and mixing layers are characterized by their mean velocity profiles with an inflection point that causes inviscid instabilities such as vortical induction where viscosity plays only a role of damping (*Ibrahim*). This is best